Hindawi
International Journal of Aerospace Engineering
Volume 2020, Article ID 2739131, 10 pages
https://doi.org/10.1155/2020/2739131

Research Article

Foreign Object Damage Performance and Constitutive Modeling of Titanium Alloy Blade

Yu Xu[1], **Li Cheng**[1], **Chang Shu**[1], **Xuan Chen**[1] and **Peiyuan Li**[1,2]

[1]*Air Force Engineering University, No. 1 Changle East Road, Baqiao District, Xi'an City, Shaanxi Province, China*
[2]*Air Force Harbin Flight Academy, 85 Nantong Street, Harbin City, Heilongjiang Province, China*

Correspondence should be addressed to Li Cheng; cheng_qiaochu@foxmail.com

Received 8 June 2019; Accepted 11 December 2019; Published 7 January 2020

Academic Editor: Paul Williams

Foreign object damage (FOD) to fan blades has been identified as one of the main factors affecting the safety of aeroengine operation. Numerical simulations are an important means of studying FOD, but the selection of the material's parameters in modeling is a key problem. In this work, a FOD test was carried out with titanium alloy blades as the sample, and the damage types suffered by the blades subjected to impacts from foreign objects under different conditions are obtained. A blade material test was carried out to obtain its parameters in terms of the Johnson-Cook material model, and finite element models of the impacting foreign objects are constructed. When comparing the test results with the simulated results, excellent correlation between them is found.

1. Introduction

During the operation of aeroengines, fan blades are vulnerable to impacts from hard objects such as stones, gravel, rivet spindles, and tire residue. As fan blades are often subjected to high-cycle and low-cycle working loads, the cracks caused by defects sprout and propagate rapidly [1–5]. Related studies have shown that the damage characteristics of foreign object damage (FOD) mainly include stress concentration associated with FOD indentation, small cracks in the damaged zone(s), plastic deformation, and residual stresses [6]. Damage from high-speed cubes impacting the leading edge of aerofoil specimens may be characterized as a mixture of notch indents, the loss of materials, material shearing, material folding, heat formation, shear bands, and microcracks, where all these characteristics can result in material fatigue which reduces the overall performance of the blade [7]. As the impact angle of the foreign object varies, its influence on the fatigue performance of the blade also varies. Meanwhile, the radius and wedge angle of the leading edge of the blade also affect the high-cycle fatigue strength of the blade after a foreign object has impacted [8]. The residual stress caused by the FOD will also adversely affect the fatigue performance of the blade. To address this, stress relief annealing treatment can strengthen the fatigue strength of a blade [9]. However, due to the small size of FOD and the large gradient of the residual stress, experimental measurements of the latter are currently not very accurate [10]. Therefore, numerical simulation techniques are needed to study the residual stresses generated by FOD. And the key of numerical simulation technology is the selection of model and model parameters.

Numerical simulation technology has been widely used in FOD research [11, 12]. Weeks et al. [13] carried out FOD tests on titanium alloy samples, and the dynamic processes resulting from the impact of steel balls on test specimens were numerically simulated using the DYMAT24 material model. Boyce et al. [14] simulated the impact process of a 3.2 mm diameter steel ball at 200 m/s and 300 m/s speeds with ABAQUS and studied the state of the residual stress after impact. Simulated results have also been compared with the results measured via the X-ray diffraction method, which show that their coincidence is good when the impact velocity is 200 m/s, but they are not ideal when the impact velocity is 300 m/s. Tranter et al. [15] used the Zerilli-Armstrong material model to simulate FOD using

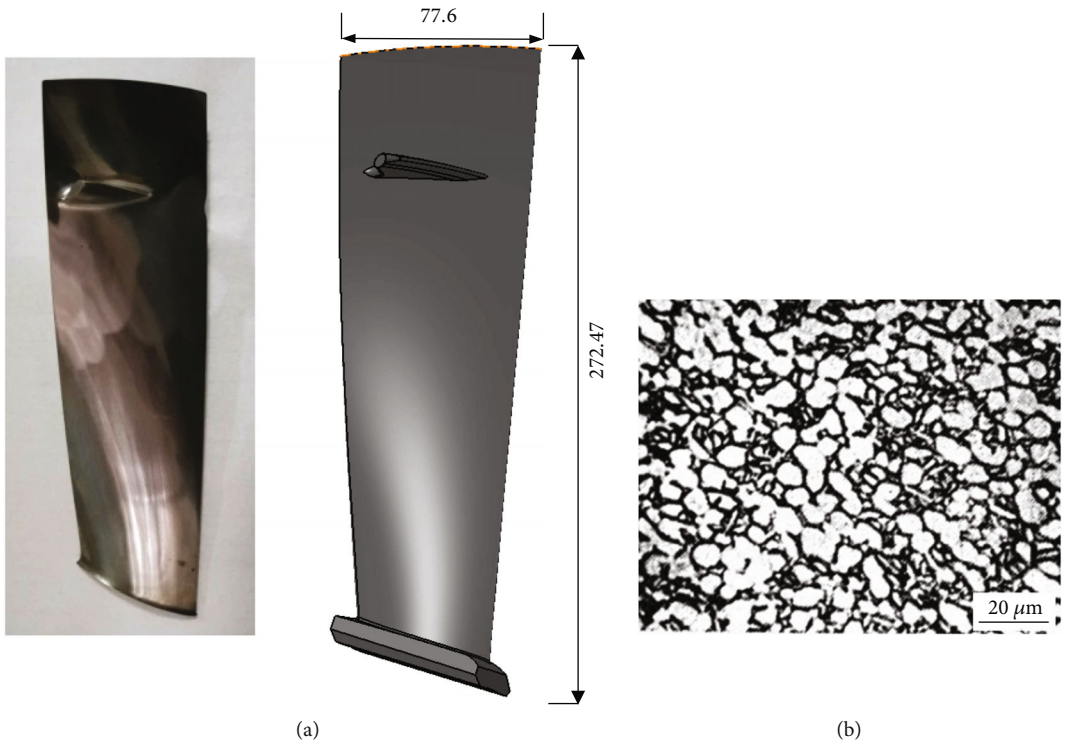

Figure 1: (a) Photographs of titanium alloy blade; (b) BT3-1 microstructure showing primary α and transformed β phases.

LS-DYNA and showed that the finite element (FE) model could simulate various impact processes. Lin et al. [16] simulated FOD impacts at 0° and at 45° angles on previously laser shock processing treated aerofoil specimens and compared the results from the simulation with those measured experimentally using high-energy synchrotron X-ray diffraction. Their results showed that the Johnson-Cook material model could be effective in predicting the dynamic response of laser shock peened specimens.

In order to accurately predict the dynamic response of FOD by numerical simulation, we need to obtain the dynamic mechanical properties of materials. One of the most widely used experimental approaches to study a material's dynamic behavior is the Split-Hopkinson Pressure Bar (SHPB), which is capable of producing strain rates up to 10^4/s [17]. While SHPB testing predominantly focuses on standard engineering materials, including concrete and sand [18], it is also often used in studying dynamic response of metal and composite [19–22]. However, only very few investigations were performed under high loading strain rates for BT3-1, which is widely used in the manufacture of aeroengine blades, and few data is currently available on dynamic constitutive behavior of it. So, it is necessary to obtain the dynamic mechanical properties of BT3-1 via SHPB tests.

The aim of this study was to explore the foreign object damage performance of titanium alloy blades and obtain Johnson-Cook constitutive model parameters of the blade material. A FOD test was carried out to obtain the damage type suffered by the blades subjected to impacts from foreign objects under different conditions. Stress-strain curves are obtained for the blade materials via a SHPB experiment, and an empirical constitutive material model based on the Johnson-Cook law is derived. The Johnson-Cook constitutive model parameters are corrected and verified by comparing the simulation results with the FOD test results.

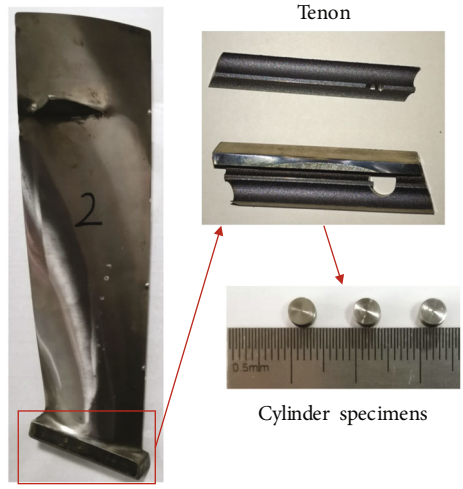

Figure 2: Specimens used in the SHPB test.

2. Experimental Measurements

2.1. Materials and Specimens. The titanium alloy blades installed in the first stage of the turbine fan engine were taken as the specimens, as shown in Figure 1(a). The material of the blades was BT3-1 titanium alloy, which is widely used in the aerospace industry to manufacture engine compressor disks, blades, rings, and fasteners. The microstructure of BT3-1 was equiaxed and consisted of a primary $\alpha + \beta$ phase, where the

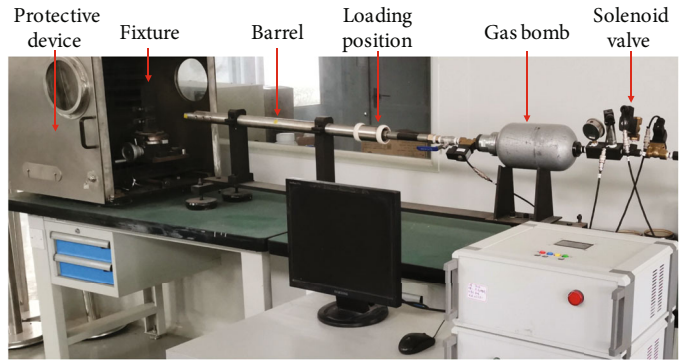

Figure 3: Gas gun device.

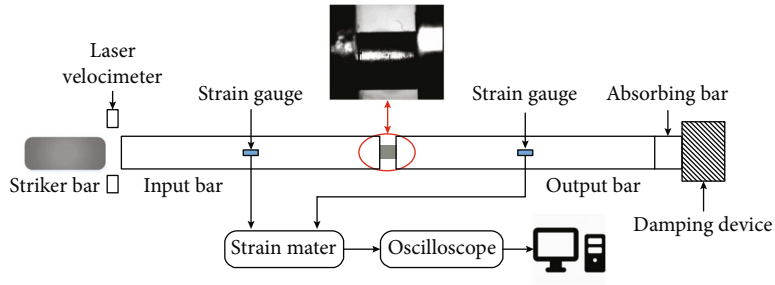

Figure 4: Schematic of the SHPB test equipment.

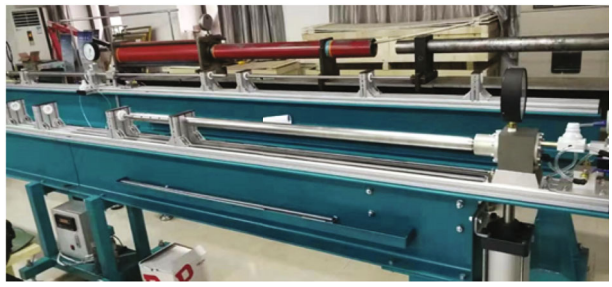

Figure 5: Practicality picture of the SHPB test equipment.

content of primary α was about 50%, and there was a large number of equiaxed secondary α phases, as shown in Figure 1(b). The projectile was a sphere with a diameter of 3 mm, which was manufactured GCR15 steel. The average hardness of the sphere was measured to be 64 (Rockwell C). All tests performed in this paper used projectiles of the same design.

The strain rate of the blade material can be as high as $10^6\ s^{-1}$ when an object impacts the blade in a real FOD event. In order to accurately establish a three-dimensional (3D) FE model of FOD, it is necessary to select the model and its parameters correctly. And the mechanical properties of the blade materials at high strain rates must be obtained to determine the model parameters. Therefore, a dynamic test was conducted on a SHPB apparatus to obtain the mechanical properties of titanium alloy blades at different strain rates. In order to obtain accurate dynamic mechanical properties of the blade's materials, the tenon part of the blade was cut and used to manufacture the specimens. The experiments

Table 1: The protocol for FOD tests.

Impactor strike angle	Impact velocity (m/s)	Projectile size (mm)	Impact position
30° 60°	80–350	3	Leading edge of the blade

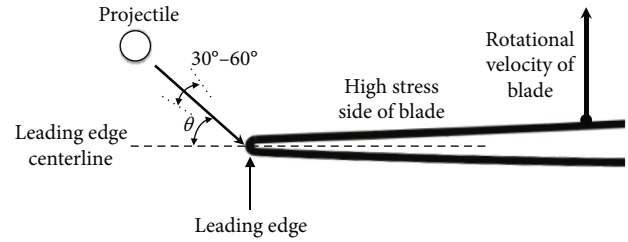

Figure 6: Schematic showing the orientations of the impacting sphere.

were performed using cylindrical specimens of the material with a size of $\Phi 4 \times 4$ mm, as shown in Figure 2.

2.2. FOD Test Device. To mimic the FOD damage conditions that might occur in service from ingested particles impacting at high velocities and strain rates, the specimens were impacted ballistically using steel ball projectiles via a 10 mm bore compressed gas gun. When air is used as medium, the gas gun was able to accelerate the steel spheres to speeds from 0 m/s to 300 m/s. When helium is used to accelerate the ball, the gas gun can accelerate the steel ball to 360 m/s. A structural drawing of the gas gun is shown in Figure 3.

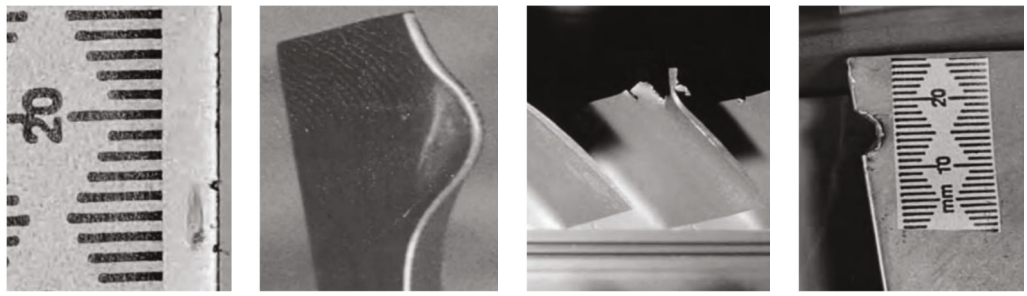

(a) "Nicked" (b) "Dented" (c) "Torn" (d) "Piece out"

Figure 7: Types of damage.

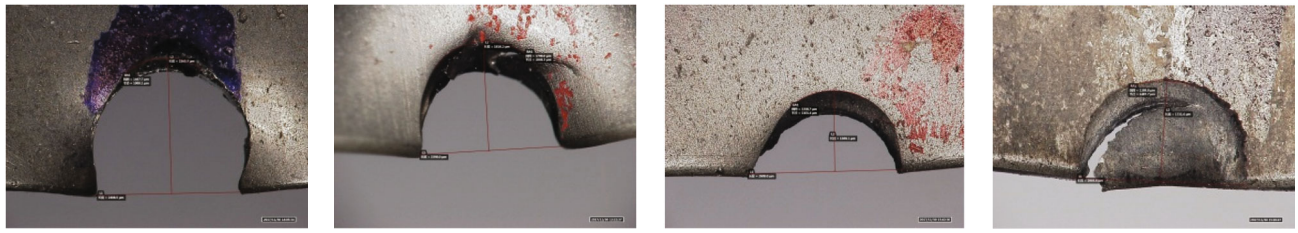

(a) 350 m/s "piece out" (b) 280 m/s "piece out" (c) 200 m/s "piece out" (d) 170 m/s "torn"

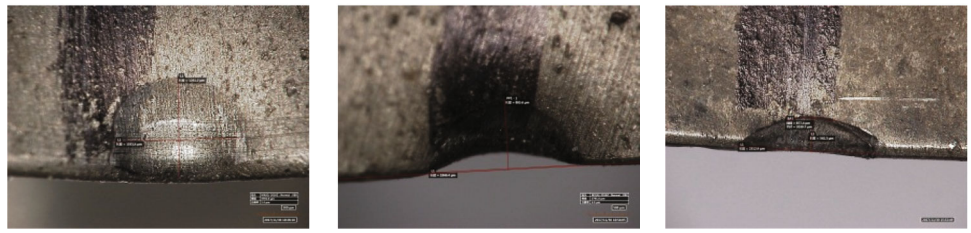

(e) 140 m/s "dented" (f) 120 m/s "dented" (g) 100 m/s "dented"

Figure 8: The typical damage of blade under 60° impacts.

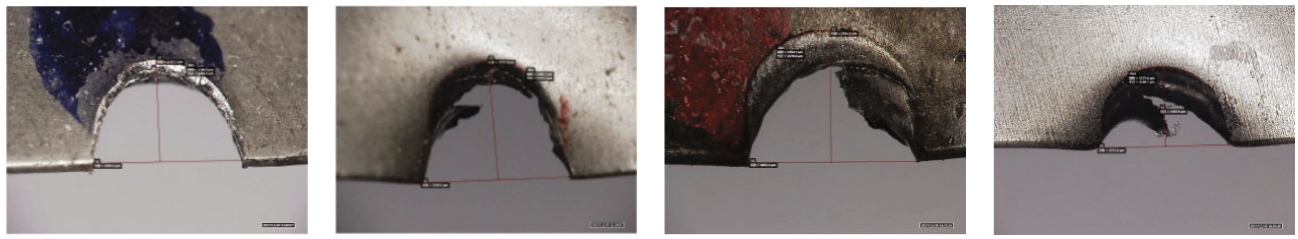

(a) 350 m/s "piece out" (b) 280 m/s "piece out" (c) 200 m/s "torn" (d) 160 m/s "torn"

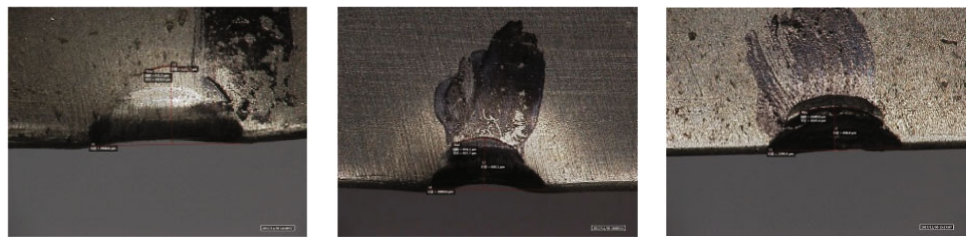

(e) 140 m/s "dented" (f) 120 m/s "dented" (g) 100 m/s "nicked"

Figure 9: The typical damage of blade under 30° impact.

The launch speed of the steel ball was varied by changing the air pressure. The steel balls were loaded into a nylon sabot, where the sabot was captured at the exit of the gun barrel by a sabot separator. This allowed the balls to propagate forward and impact the target directly. The actual impact speed was measured by a velocimetry system installed

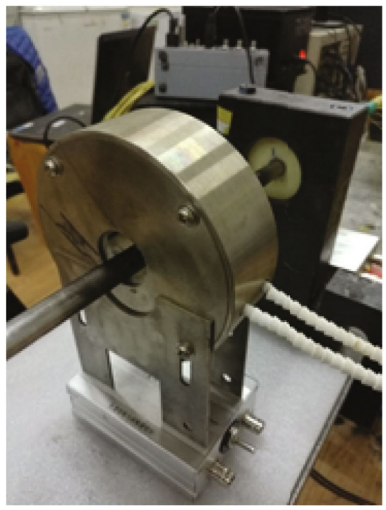

Figure 10: Heating furnace.

between the gun muzzle and the target. The gas gun test system adopted a support structure, where a sheller was installed at the exit of the barrel. The details of the damage simulation technique are described elsewhere [8].

2.3. SHPB Test Device. The SHPB apparatus consisted of a striking system, an input bar, an output bar, a momentum trap bar, and a data acquisition system, as shown in Figures 4 and 5. Both the diameters and the lengths of the input and output bars were the same, which were 14 mm and 1500 mm, respectively. The bars were made of titanium alloy with a Young's modulus E of 110 GPa and a density ρ of 4400 kg/m^3. A gas gun was used to launch the striker bar. The impact between the striker bar and the input bar generated a longitudinal pulse wave which was instantly applied to the input bar. The incident, reflected, and transmitted strain waves were measured by strain gauges mounted at the middle position of the input and output bars.

3. Results

A series of impact tests were conducted on the titanium alloy blades, where the protocols of the FOD tests are listed in Table 1. In this study, two angles (30° and 60°) were used. Previous studies [23] have shown that the incident angle of a foreign object impacting a blade is within the range of 30°–60° with respect to the centerline of the blade, as portrayed in Figure 6.

Previous studies [23] have shown that FOD mostly occurs at the edge of a blade, especially at the leading edge, where the damage at this position has a significant impact on the fatigue performance of the blade. As such, the blade edge was taken as the impact position. The impact speed mainly depends on the engine speed. The maximum speed of the fan rotor is about 10,098 rev/min. As such, the linear speed ranges of the blade root and tip were 57.90–192.99 m/s and 141.69–472.31 m/s, respectively. Therefore, different speeds in the range of 100 m/s to 350 m/s were selected in this study.

The macroscopic damage morphology of each FOD was observed. According to the previously reported classifications of FOD damage [9, 10], it was found that the main damage types suffered by the blades were "nicked," "dented," "torn," and "piece out," as shown in Figure 7. "Nicked" implies a relatively short, sharp indentation, usually occurring at the leading or trailing edges of the blade, where a small amount of material is removed. "Dented" is an indentation with a rounded bottom, which usually appears on the leading/trailing edge of the blade. Raw material is displaced, but it is seldom separated. "Torn" is a phenomenon whereby the material is separated but does not completely fall off. "Piece out" infers that a chuck of material has been removed from the leading/trailing edge. "Nicked" and "dented" usually appear in low-velocity impacts, while "piece out" usually appears during high-velocity impacts.

The results of the FOD impact on the leading edge of the blade for 60° impacts are shown in Figure 8. The steel ball impacted the leading edge of the blade at speeds of 100–350 m/s. It can be seen that in the impact velocity range of 200–350 m/s, the type of damage was mainly "piece out." In the impact velocity range of 100–140 m/s, the damage type was mainly "dented." "Torn" appeared less frequently, where it only appeared when the impact velocity was about 170 m/s and did not appear in the other impact velocity. The range of speeds at which "torn" features appeared was small, and it is between the speeds at which "dented" and "piece out" appeared. Hence, "torn" can be regarded as a transitional damage type between "dented" and "piece out."

The results of the FOD on the leading edge of the blade for 30° impacts are shown in Figure 9. As the impact speed increased, the three types of damage ("dented," "torn," and "piece out") appeared one after another. However, compared with the impact angle of 60°, where the range of speeds at which the "torn" feature appears was 160–200 m/s, under 30° impacts, the speed range was 140–200 m/s.

Multiple strain rates were applied to obtain the dynamic responses of the specimens under different testing temperatures of 20°C, 200°C, and 400°C. Testing at high temperatures is important as the temperature of the material will increase due to the impact process. The testing temperatures were achieved by using a heating furnace where the temperature was monitored with rapid response thermocouples, as shown in Figure 10.

Since the strain rate of 10^6 s^{-1} could not be reached by the SHPB experimental device, we selected a high strain rate (6500 s^{-1}), medium strain rate (3000 s^{-1}), and low strain rate (1000 s^{-1}) according to the maximum strain rate achieved by the SHPB experimental device to conduct the experiment so as to ensure the accuracy of constitutive parameter fitting under different strain rates. True stress-strain curves were obtained at three different strain rates (1000 s^{-1}, 3000 s^{-1}, and 6500 s^{-1}) for the cylinder specimens. During each test condition, three groups of data were measured to ensure the reliability of test data. The average stress-strain curves were calculated according to three groups of true stress-strain curves under different test conditions, as shown in Figure 11.

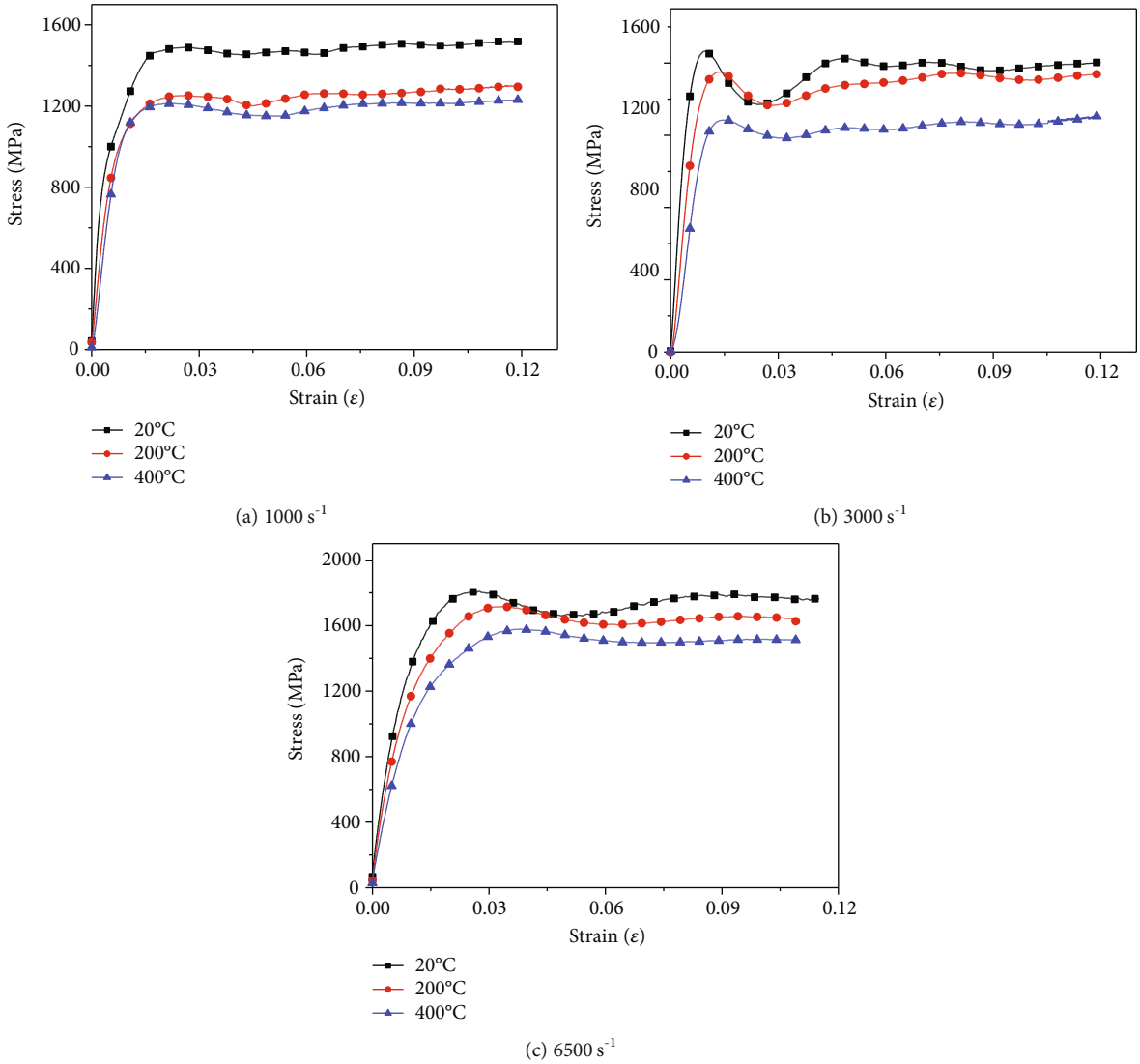

Figure 11: Stress-strain relation of specimens.

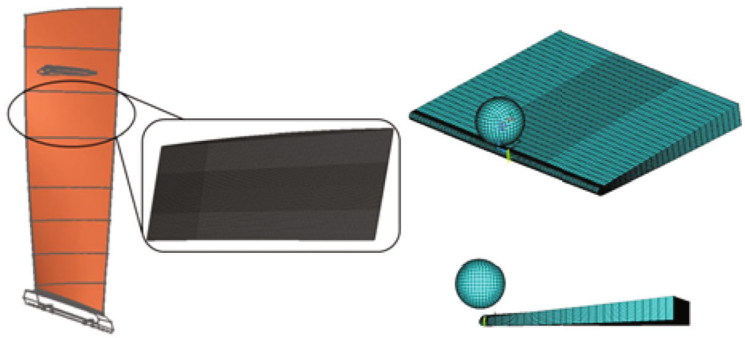

Figure 12: Finite element model of the blade and sphere.

4. Discussion

In order to predict the dynamic response of the blade at 30° and 60° impacts, numerical simulations were carried out using the finite element code LS-DYNA. Figure 12

Table 2: Johnson-Cook material constants for BT3-1.

A (MPa)	B (MPa)	C	m	n
1140	986	0.03	1.29	0.95

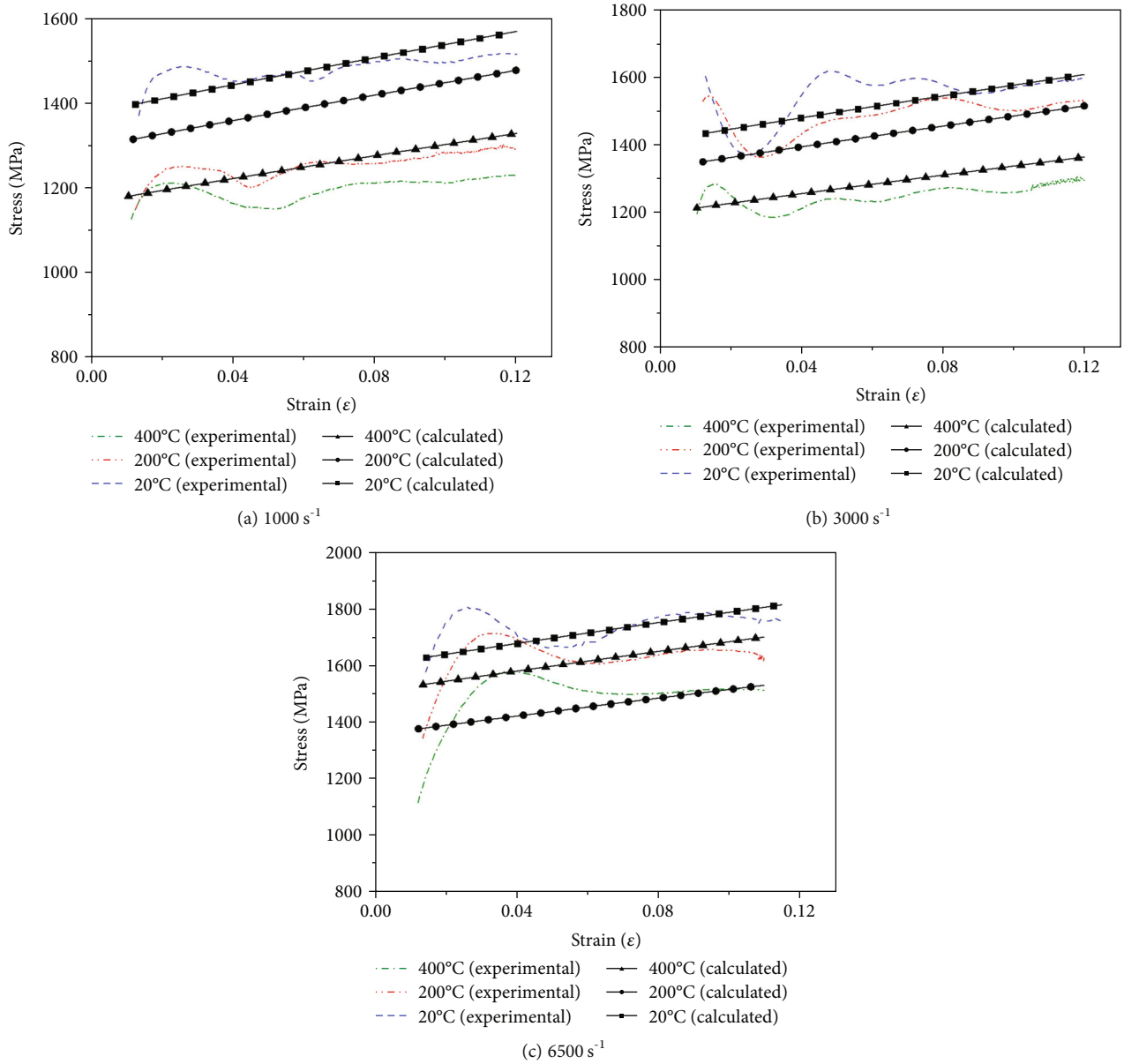

Figure 13: Comparison of calculation curves and test results.

shows a typical finite element model of the steel ball and the blade. If the whole blade is meshed, the number of meshes is too large. Therefore, only a part of the blade was intercepted and hence meshed. The steel sphere was modelled as a rigid body, and the blade as a deformable body. Due to the thinness of the small leading edge, friction between the steel sphere and the blade was assumed to be negligible. The boundary conditions of the numerical model are fixed at both ends of the blade. The upper and lower boundaries of the blade were restrained with respect to all degrees of freedom. Material failure may occur due to material failure during high-speed impact. The failed unit needs to be deleted, so the contact type selected is face-to-face contact ESTS. Hexahedral elements (SOLID 164) were considered in all simulations carried out in the present study. Due to the fact that the blade experienced significant plastic deformation and fracturing in the contact zone, the mesh density in this region was highly refined. The minimum size of each element in the contact region was between 0.10 and 0.15 mm. The mesh size of other areas on the blade is 0.5 mm, and the blade has a total of 18,750 elements. The sphere adopts the mapping grid division method, with a mesh size of 0.5 mm and a total of 1655 elements.

Table 3: Johnson-Cook failure parameters.

D_1	D_2	D_3	D_4	D_5
-0.09	0.27	0.48	0.01	3.87

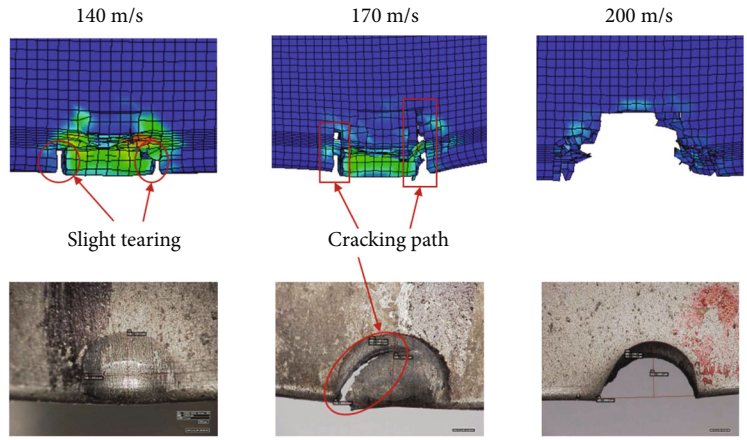

Figure 14: Comparison of experimental results with simulation results.

The Johnson-Cook constitutive relation and its associated failure criterion were adopted in this work. The Johnson-Cook constitutive model is given by Johnson and Cook [24]:

$$\sigma_y = \left(A + B\varepsilon_p^n\right)\left(1 + C\ln\dot{\varepsilon}^*\right)(1 - T^{*m}), \quad (1)$$

where σ_y is the flow stress of the material. A, B, n, C, and m are experimentally determined constants, where A is the initial yield strength, B and n represent the effects of strain hardening, C is the strain rate sensitivity coefficient, and m is the thermal softening coefficient. $\dot{\varepsilon}^*$ is the dimensionless equivalent plastic strain rate, and T^* is the dimensionless temperature.

Based on our dynamic test data of the blade materials, the parameters of the Johnson-Cook constitutive model were estimated with the Levenberg-Marquardt algorithm [25]. The estimated results are shown in Table 2.

Figure 13 compares the calculated curves with the true stress-strain curves. It can be seen that for strain rates of $3000\,s^{-1}$ and $6500\,s^{-1}$, the calculated curves were in good agreement with the experimental results. However, there were some errors between the fitted curves and the experimental results under some conditions, such as 200°C and $1000\,s^{-1}$, but in general, the calculated curves and the experimental results tended to agree.

A dynamic failure model that uses the Johnson-Cook shear failure criterion was applied to model the material losses during the impact process. The Johnson-Cook failure criterion is defined as

$$\varepsilon_f = (D_1 + D_2\exp(D_3\sigma^*))\left(1 + D_4\ln\dot{\varepsilon}^*\right)(1 + D_5T^*), \quad (2)$$

where D_1–D_5 are failure parameters measured at or below the transition temperature, T_r. The data in this paper are not enough to calculate the failure parameters of the BT3-1 alloy, so the failure parameters of the Ti-6Al-4V alloy taken from the literature [26] were used instead, which are summarized in Table 3.

Table 4: The modified Johnson-Cook material parameters.

A (MPa)	B (MPa)	C	m	n
1140	1214	0.035	1.29	0.95

The Johnson-Cook material constants together with the Johnson-Cook failure parameters $D_1 - D_5$ given in Table 3 were used to simulate a 60° impact, where the results are shown in Figure 14. It can be seen that under impact speeds of 140 m/s, 170 m/s, and 200 m/s, "dented," "torn," and "piece out" features appeared, respectively, which are similar to the experimental results.

However, there are still some differences in the details of the numerical simulation results and experimental results. For example, when the impact speed was 140 m/s, the numerical simulation results showed slight tearing, while at an impact speed of 170 m/s, the results of the numerical simulation were substantially cracked in a direction perpendicular to the edge of the blade, while the results of the test were cracked along the edge of the indentation. As there was some disconformity in the results, it was necessary to modify the Johnson-Cook material parameters so that the FE simulation could accurately predict the results of the experimental FOD test.

The accurate determination of the material's parameters at high strain rates in the Johnson-Cook model is of vital importance for the FE simulations. In this work, we adopted a "trial-and-error" approach to obtain these parameters. We constantly compared the experimental results with the numerical simulation results through iterative FE analyses. If the numerically simulated results did not meet the test results, the constant parameters were adjusted within the error tolerance range, and the influence of each parameter on the damage was analyzed. We set the range of parameter adjustment based on the Johnson-Cook model parameters of titanium alloy studied by other scholars. The adjustment value should not exceed the normal range of constitutive model parameters of titanium alloy. The constitutive parameters have physical meaning. Therefore, according to the numerical simulation results and the physical meaning of the parameters, first, manually adjust one parameter and

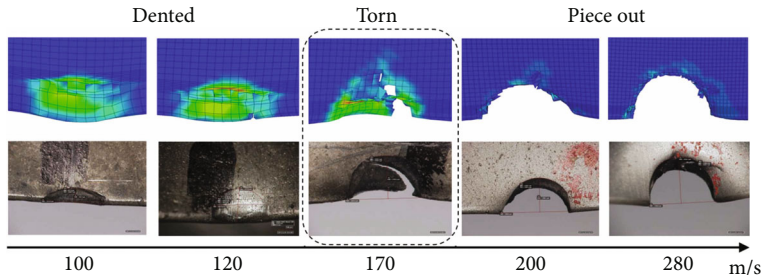

Figure 15: Comparison of experimental results with simulation results for 60° impact.

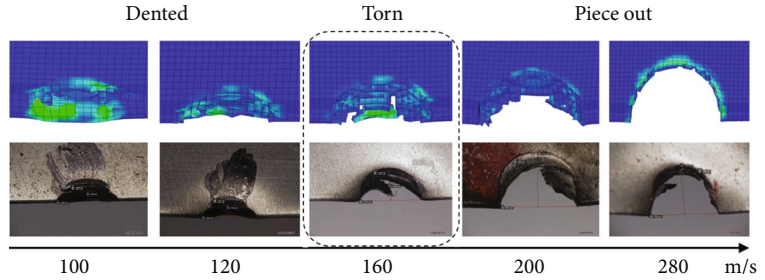

Figure 16: Comparison of experimental results with simulation results for 30° impact.

then use the Levenberg-Marquardt algorithm to fit the remaining parameters. After many corrections and verifications, the results of the numerical simulation finally coincided with the test results. The modified Johnson-Cook parameters are shown in Table 4.

Based on the modified parameters, FE analyses were carried out at different speeds under 60° impacts. The simulated results at different impact speeds were in good agreement with the experimental results, as shown in Figure 15.

Figure 16 compares the FE simulation results and test results under 30° impacts. It can be seen that the simulated results are also in good agreement with the experimental results, further indicating that the FE model can effectively predict the FOD test results.

5. Conclusions

In this paper, FOD tests were carried out to study the damage types suffered by blades subjected to foreign object impacts. The Johnson-Cook model parameters were estimated through SHPB tests, where 3D FE models were developed to simulate foreign objects impacting upon the leading edge of the blade. In our analysis, the Johnson-Cook material parameters were corrected by comparing the results from the simulation with the experimental FOD test results.

Tearing occurs at 30° and 60° impacts, and the range of speeds at which the "torn" feature appears is small. The "torn" feature usually appears between the "dented" and "piece out" features, so the former can be regarded as a transitional damage type between them.

The Johnson-Cook material parameters of the BT3-1 alloy obtained from the SHPB test were used to develop the 3D FE models; however, the model was inaccurate in predicting the results of the impacts. Therefore, the Johnson-Cook material parameters were corrected by comparing the results from the simulations with the FOD test results, which seemed to be effective in predicting the dynamic response of blades for 30° and 60° impacts.

Data Availability

The raw data used to support the findings of this study have not been made available because the data also forms part of an ongoing study.

Conflicts of Interest

The authors declare that there is no conflict of interest regarding the publication of this paper.

Acknowledgments

This study was supported by the National Basic Research Program of China (973 Program) (Grant No. 2015CB057400), the National Natural Science Foundation of China under the contract No. 11402302, the Shanxi Natural Science Foundation under the contract No. 2016JQ1031, and the China Postdoctoral Science Foundation under the contract No. 2016M592923.

References

[1] T. Nicholas, J. P. Barber, and R. S. Bertke, "Impact damage on titanium leading edges from small hard objects," *Experimental Mechanics*, vol. 20, no. 10, pp. 357–364, 1980.

[2] J. R. Nicholls, Y. Jaslier, and D. S. Rickerby, "Erosion and foreign object damage of thermal barrier coatings," *Materials Science Forum*, vol. 251-254, pp. 935–948, 1997.

[3] X. Chen, R. Wang, N. Yao, A. G. Evans, J. W. Hutchinson, and R. W. Bruce, "Foreign object damage in a thermal barrier

system: mechanisms and simulations," *Materials Science and Engineering: A*, vol. 352, no. 1–2, pp. 221–231, 2003.

[4] J. Calcaterra, "Appendix G - experimental and analytical simulation of FOD," in *High Cycle Fatigue: A Mechanics of Materials Perspective*, pp. 558–599, Springer, Berlin Heidelberg, 2006.

[5] L. Liu, Z. Zhao, W. Chen, and G. Luo, "Ballistic impact behaviour of stiffened aluminium plates for gas turbine engine containment system," *International Journal of Crashworthiness*, vol. 22, no. 5, pp. 467–478, 2017.

[6] J. O. Peters and R. O. Ritchie, "Foreign-object damage and high-cycle fatigue: role of microstructure in Ti-6Al-4V," *International Journal of Fatigue*, vol. 23, no. 1, pp. 413–421, 2001.

[7] S. Spanrad and J. Tong, "Characterisation of foreign object damage (FOD) and early fatigue crack growth in laser shock peened Ti–6Al–4V aerofoil specimens," *Materials Science and Engineering: A*, vol. 528, no. 4, pp. 2128–2136, 2011.

[8] D. Nowell, P. Duó, and I. F. Stewart, "Prediction of fatigue performance in gas turbine blades after foreign object damage," *International Journal of Fatigue*, vol. 25, no. 9–11, pp. 963–969, 2003.

[9] T. Nicholas, S. Thompson, W. Porter, and D. Buchanan, "Comparison of fatigue limit strength of Ti–6Al–4V in tension and torsion after real and simulated foreign object damage," *International Journal of Fatigue*, vol. 27, no. 10-12, pp. 1637–1643, 2005.

[10] P. Duó, J. Liu, D. Dini, M. Golshan, and A. M. Korsunsky, "Evaluation and analysis of residual stresses due to foreign object damage," *Mechanics of Materials*, vol. 39, no. 3, pp. 199–211, 2007.

[11] Z. Zhenhua, L. Lulu, C. Wei, and L. Gang, "Numerical simulation methodology of multi-layer Kevlar 49 woven fabrics in aircraft engine containment application," *International Journal of Crashworthiness*, vol. 24, no. 1, pp. 86–99, 2018.

[12] H. Tan, L. Liu, Y. Guan, W. Chen, and Z. Zhao, "A simplified delamination modelling methodology for triaxial braided composites with macro-scale solid finite-element models," *International Journal of Crashworthiness*, vol. 24, no. 1, pp. 54–70, 2018.

[13] C. Weeks, P. Bastnagel, T. Cook, R. Daiuto, and J. Delp, "FOD analytical modelling-FOD event modelling," *United States Air Force Technical Report, Improved High Cycle Fatigue Life Prediction, Appendix 5E, AFRL-ML-WP-TR-2001-4159*, Wright-Patterson AFB, OH, 2001.

[14] B. L. Boyce, X. Chen, J. W. Hutchinson, and R. O. Ritchie, "The residual stress state due to a spherical hard-body impact," *Mechanics of Materials*, vol. 33, no. 8, pp. 441–454, 2001.

[15] P. H. Tranter, P. J. Gould, and G. F. Harrison, "Laboratory simulation and finite element modelling of aerofoil impact damage," in *Proceedings of the 8th National Turbine Fatigue High Cycle Fatigue Conference*, Monterey, CA, USA, 2003.

[16] B. Lin, S. Zabeen, J. Tong, M. Preuss, and P. J. Withers, "Residual stresses due to foreign object damage in laser-shock peened aerofoils: simulation and measurement," *Mechanics of Materials*, vol. 82, pp. 78–90, 2015.

[17] B. A. Gama, S. L. Lopatnikov, and J. W. Gillespie, "Hopkinson bar experimental technique: a critical review," *Applied Mechanics Reviews*, vol. 57, no. 4, pp. 223–250, 2004.

[18] B. E. Martin, W. Chen, B. Song, and S. A. Akers, "Moisture effects on the high strain-rate behavior of sand," *Mechanics of Materials*, vol. 41, no. 6, pp. 786–798, 2009.

[19] H. Zhou, B. Sun, and B. Gu, "Responses of 3D four-directional and five-directional circular braided composite tubes under transverse impact," *International Journal of Crashworthiness*, vol. 21, no. 4, pp. 353–366, 2016.

[20] L. Ninan, J. Tsai, and C. T. Sun, "Use of split Hopkinson pressure bar for testing off-axis composites," *International Journal of Impact Engineering*, vol. 25, no. 3, pp. 291–313, 2001.

[21] L. Mingshuang, L. Yulong, X. Fei, X. Zejian, and C. Laifei, "Dynamic compressive mechanical properties and a new constitutive model of 2D-C/SiC composites," *Materials Science and Engineering: A*, vol. 489, no. 1-2, pp. 120–126, 2008.

[22] C. Xuan and L. Yulong, "Dynamic tensile behavior of two-dimensional carbon fiber reinforced silicon carbide matrix composites," *Materials Science and Engineering: A*, vol. 528, no. 22-23, pp. 6998–7004, 2011.

[23] T. Nicholas, *High Cycle Fatigue: A Mechanics of Materials Perspective*, Elsevier Ltd, 2006.

[24] G. R. Johnson and W. H. Cook, "Fracture characteristics of three metals subjected to various strains, strain rates, temperatures and pressures," *Engineering Fracture Mechanics*, vol. 21, no. 1, pp. 31–48, 1985.

[25] Z. Guangcheng, *Nonlinear Optimization Method*, Higher Education Press, 2005.

[26] G. Kay, *Failure modeling of titanium 6Al–4V and aluminum 2024-T3 with the Johnson–Cook material model*, 2003, *FAA report, DOT/FAA/AR-03/57*.